ACS APPLIED MATERIALS & INTERFACES

Research Article

www.acsami.org

C_{60}-Decorated CdS/TiO_2 Mesoporous Architectures with Enhanced Photostability and Photocatalytic Activity for H_2 Evolution

Zichao Lian,[†] Pengpeng Xu,[†] Wenchao Wang, Dieqing Zhang,* Shuning Xiao, Xin Li, and Guisheng Li*

Key Laboratory of Resource Chemistry of Ministry of Education, Shanghai Key Laboratory of Rare Earth Functional Materials, College of Life and Environmental Science, Shanghai Normal University, Shanghai, 200234, People's Republic of China

Supporting Information

ABSTRACT: Fullerene (C_{60}) enhanced mesoporous CdS/TiO_2 architectures were fabricated by an evaporation induced self-assembly route together with an ion-exchanged method. C_{60} clusters were incorporated into the pore wall of mesoporous CdS/TiO_2 with the formation of C_{60} enhanced CdS/TiO_2 hybrid architectures, for achieving the enhanced photostability and photocatalytic activity in H_2 evolution under visible-light irradiation. Such greatly enhanced photocatalytic performance and photostability could be due to the strong combination and heterojunctions between C_{60} and CdS/TiO_2. The as-formed C_{60} cluster protection layers in the CdS/TiO_2 framework not only improve the light absorption capability, but also greatly accelerated the photogenerated electron transfer to C_{60} clusters for H_2 evolution.

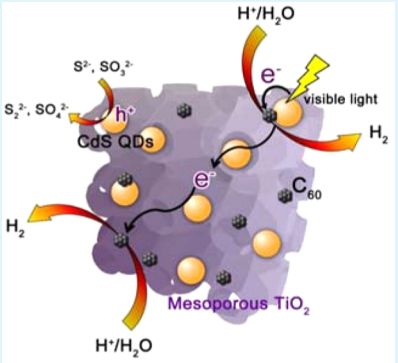

KEYWORDS: *C_{60}, CdS, TiO_2, photostability, photocatalytic, H_2*

1. INTRODUCTION

Since Fujishima and Honda had reported that hydrogen evolution could be obtained through photoelectrochemical water-splitting by using TiO_2 as electrodes,[1−4] the semiconductor-based photocatalysis induced water-splitting route for hydrogen evolution has been recognized as one of the most effective methods for solving the energy crisis.[5] Also, cadmium sulfide (CdS) with a band gap of around 2.4 eV matches well with the visible part of solar-light spectra and exhibits excellent photocatalytic activity because of its highly effective absorption of solar energy.[6] Thus, it has been applied in different kinds of fields such as optoelectronics,[7] solar cells,[8] chemical sensors,[9] and photocatalysis.[10] However, its photocorrosion effect gas greatly limited its wide application.

In addition, our earlier work proved that ordered mesoporous TiO_2 CdS with quantum dots (QDs) implanted into its framework could be applied in the treatment of both water and air purification under visible-light irradiation.[11] Nevertheless, there still exist some problems in such photocatalytic systems, including the low photocatalytic activity resulting from the low electronic conductivity, low quantum efficiency, and the inherent photocorrosion problem drawback for CdS-based photocatalysts.[12,13] As is already known, the sulfide ion could easily be oxidized by photogenerated holes, and cadmium ions could be reduced by the photoinduced electrons. Such photocorrosion effects lead to the instability of CdS, seriously prohibiting its practical application. Thus, it is key to seek a new approach to inhibit the photocorrosive effect to the CdS nanoparticles via choosing a surface-modification route involving loading a thin amorphous-carbon layer around CdS,[14] or forming a heterojunction[15] and a Z-scheme[16] to accelerate the photoinduced electron transfer. Thus, carbon nanostructured materials such as activated carbon, multiwalled carbon nanotubes,[17−20] single-walled carbon nanotubes (SWCNTs),[21,22] fullerenes (C_{60}),[23] and reduced graphene oxide (rGO)[24−27] give us a new space in which to design nanocomposites with excellent photocatalytic performance in recent years. Among these carbon nanostructured materials, C_{60} has gained a lot of attention for its novel properties owing to its special delocalized conjugated structures.[27] The most important role of C_{60} in electron-transfer processes lies in that it could serve as an excellent electron acceptor. This efficiently increases the photogenerated charge separation and decreases the rate of charge recombination,[28] thus enhancing the photocatalytic activity. Therefore, combining photocatalysts with fullerene could provide an excellent route for obtaining rapidly photogenerated charge separation via facilitating electron transfer.[29,30] Also, C_{60} molecules could be regarded as the antiphotocorrosion agent.[31] Given those advantages, it is highly necessary to implant C_{60} into the mesoporous framework of CdS/TiO_2 composites to enhancie the activity and stability.

Herein, we report the fabrication of C_{60}-decorated CdS QDs sensitized mesoporous TiO_2 photocatalysts via an evaporation induced self-assembly (EISA), together with an ion-exchange route.[11] CdS QDs and C_{60} clusters were well embedded into the framework of the well-ordered mesoporous TiO_2 photo-

Received: October 12, 2014
Accepted: February 6, 2015
Published: February 6, 2015

DOI: 10.1021/am5088665
ACS Appl. Mater. Interfaces 2015, 7, 4533−4540

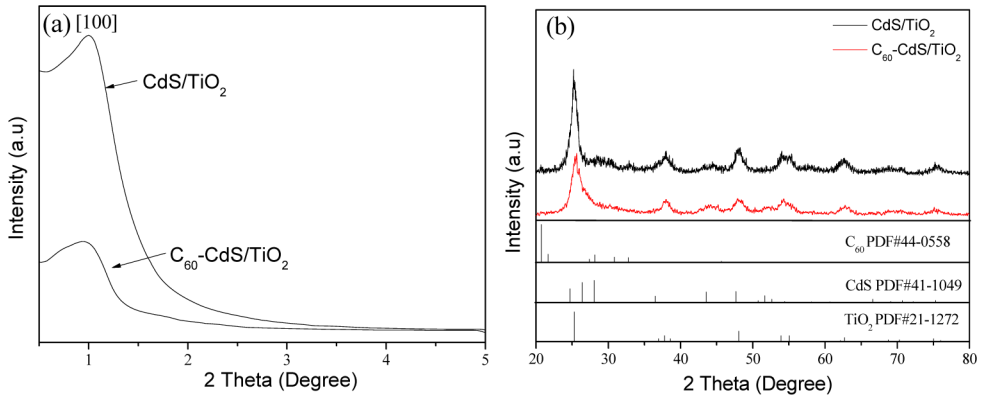

Figure 1. Small-angle X-ray diffraction (SXRD) (a) and wide-angle X-ray diffraction (WXRD) (b) of CdS/TiO_2 and C_{60}−CdS/TiO_2.

catalyst. The C_{60} cluster protection layers were distributed on the surface of both CdS and TiO_2. Such layers were favorable for enhancing the photocatalytic performance in H_2 evolution with excellent stability, owing to the photogenerated electron transfer on the C_{60} clusters.

2. EXPERIMENTAL SECTION

2.1. Sample Preparation. *2.1.1. C_{60}−CdO/TiO_2.* Poly(alkyleneoxide) block copolymer (Pluronic F-127, Sigma-Aldrich, 1.5 g) was dissolved in 19 mL of ethanol (EtOH) containing 0.21 g $Cd(NO_3)_2{\cdot}4H_2O$ and different amounts of transparent purplish red C_{60}−toluene solution. Then, 0.015 mol titanium tetrachloride (Shanghai Aladdin) was added into the above solution with vigorous stirring for 0.5 h. The mass ratio of C_{60}/TiO_2 was changed from 0.25 to 1.5 wt %. The formed solution was then transferred to an open Petri dish, and gelled at 40 °C in an oven for 4 days. Finally, the as-prepared transparent solid gel was further calcined at 400 °C for 4 h in air.

2.1.2. C_{60}−CdS/TiO_2. 0.3 g C_{60}−CdO/TiO_2 powders were introduced in a Na_2S aqueous solution (50 mL, 0.2 M). The above solution was stirred for 10 h at room temperature. The as-obtained powders were then filtered, washed with DI water, and collected for further utiliation. For comparison, a pure ordered mesoporous TiO_2 and CdS/TiO_2 was also synthesized by the same method without Cd source or C_{60}−toluene solution addition.

2.1.3. C_{60}/CdS. 2.135 g $Cd(NO_3)_2{\cdot}4H_2O$ was dissolved in 50 mL H_2O containing transparent purplish red C_{60}−toluene solution with stirring for 24 h. The resulting precipitate was filtered, washed with water and ethanol, and dried at 80 °C for 12 h. The as-obtained products were further calcined at 400 °C for 4 h in air to obtain C_{60}/CdO powders. Then, the as-obtained C_{60}/CdO (0.3 g) was dispersed in a Na_2S aqueous solution (50 mL, 20.0 g/L) with stirring for 10 h at 80 °C. The as-obtained brown products were filtered, washed with water and ethanol three times, and dried at 80 °C for 12 h. The mass ratio of C_{60}/CdS was tuned from 0.25 to 1.5 wt %.

2.2. Characterization. Both wide and low-angle X-ray diffraction measurements were performed on a Rigacu Dmax-3C X-ray diffractometer using a parallel mode. High-resolution transmission electron microscopy (HRTEM) was measured in a JEOL-2010 at 200 kV. The TEM or HRTEM samples were prepared by grinding and dispersing the photocatalyst powders in ethanol for 20 s under ultrasonic irradiation. Carbon coated copper grids were utilized as holders for loading samples. BET surface area, pore volume, and average pore diameter of photocatalyst were measured by N_2 adsorption at −196 °C using TriStar II 3020 system by Micromeritics Instrument Corporation. The binding energies of the elements in the products were investigated by the X-ray photoelectron spectroscopy (XPS) using a PerkinElmer PHI 5000C. The contaminant carbon (C 1s = 284.6 eV) was chosen as a reference for calibrate the binding energies. The UV−vis diffuse reflectance spectra (200−800 nm) were recorded by a MC-2530 UV−vis spectrophotometer system equipped with a Labsphere diffuse reflectance accessory. $BaSO_4$ was used as a reference. Photoluminescence (PLS) emission spectra were recorded on a Varian Cary-Eclipse 500 at room temperature using 280 nm light as the excitation source. Thermogravimetric analyses (TG) were carried out on a DTG-60H thermogravimetric analyzer with a heating speed of 2 °C/min under air atmosphere.

2.3. Photoelectrochemical Measurements. The photocurrents were recorded on an electrochemical analyzer (CHI 660D Instruments, Chen Hua Instrument Co., Ltd.) in a standard three-electrode system. Platinum sheet (20 × 20 × 0.1 mm^3, 99.99%) was used as the counter electrode, and a saturated calomel electrode (SCE) was used as the reference electrode. The as-prepared samples electrode was used as the working electrode. In order to drive the photogenerated electron transfer from the working electrode to the platinum electrode, an external bias voltage (0.5 V) was loaded. For preparing the working electrode, the as-obtained photocatalyst powders (20 mg) were ground with polyethylene glycol (PEG, molecular weight 20 000, 0.01 g) and ethanol (0.5 mL) to form a slurry. Afterward, the slurry was spin-coated onto an FTO glass electrode (3 × 1 cm^2) for the formation of an active area (10 × 10 mm^2). The as-formed electrodes were further heated at 200 °C for 3 h in a ceramic plate heater. A xenon lamp (300 W, $\lambda > 420$ nm) was used as the visible-light source, and the photoelectrochemical cell was positioned 10 cm away from the xenon lamp. Na_2SO_4 aqueous solution (0.5 mol/L) was used as the electrolyte.

2.4. Activity Test. *2.4.1. Photocatalytic H_2 Generation.* Hydrogen production by photocatalytic water-splitting was carried out at room temperature in a three flat-bottomed flask reaction cell (100 mL) sealed with aboral rubber plugs. Typically, ordered mesoporous C_{60}−CdS/TiO_2 photocatalyst (50 mg) was suspended in a Na_2S−Na_2SO_3 aqueous solution (80 mL, 0.25 M for Na_2S, 0.25 M for Na_2SO_3). Before light-irradiation, nitrogen flow was introduced into the photocatalyst suspension to remove the dissolved O_2. Four low power UV-LEDs (3 W, 420 nm) (Shenzhen LAMPLIC Science Co. Ltd., China) were utilized as the light source for driving the photocatalytic H_2 evolution. In four different directions, all LEDs were positioned away from the reactor with a distance of ca. 1 cm. Each UV-LED possessed a focused intensity (ca. 6 $mW{\cdot}cm^{-2}$) and areas (ca. 1 cm^2) on the reaction flask. For keeping the photocatalysts in suspension status, vigorous magnetic stirring was maintained during the photocatalytic reaction. 0.5 mL of gas was sampled intermittently after 1 h of photocatalytic reaction. The evolved H_2 amount was determined using a gas chromatograph (GC9800 (N), Shanghai Ke Chuang Chromatograph Instruments Co. Ltd., China, TCD, nitrogen as carrier gas, and a 5 A molecular sieve column).

The apparent quantum efficiency (QE) was very important to evaluate the photocatalytic performance. And the QE was calculated according to eq 1:[32]

DOI: 10.1021/am5088665
ACS Appl. Mater. Interfaces 2015, 7, 4533−4540

$$\mathrm{QE}[\%] = \frac{\text{number of reacted electrons}}{\text{number of incident photons}} \times 100 = \frac{\text{number of evolved } H_2 \text{molecules} \times 2}{\text{number of incident photons}} \times 100 \quad (1)$$

3. RESULTS AND DISCUSSION

For investigating the crystalline phase and mesostructure of the as-formed C_{60}−CdS/TiO_2 samples, both wide-angle X-ray diffraction (WXRD) and small-angle X-ray-diffraction (SXRD) were applied in the present work. The small-angle XRD patterns demonstrated that both CdS/TiO_2 and C_{60}−CdS/TiO_2 samples exhibited strong peaks indicative of (100) diffraction, suggesting that the samples possessed a highly ordered 2D hexagonal mesoporous structure (p6 mm), as shown in Figure 1a.[33,34] It revealed that the in situ introducing C_{60} and the transfer from CdO to CdS did not destroy the framework of the ordered mesoporous structure, although a slight decrease of (100) diffraction peak was observed upon coupling C_{60} with CdS/TiO_2. Wide-angle XRD of CdS/TiO_2 and C_{60}−CdS/TiO_2 samples indicated the diffraction peaks at 2θ of 25.3°, 36.9°, 38.2°, 38.6°, 48.1°, 53.5°, 55.6°, 62.7°, and 75.0° of an anatase−TiO_2 structure (JCPDF 21−1272) in Figure 1b. Meanwhile, there was an additional diffraction peak at 2θ of 43.6°, ascribed to the (110) crystal plane of hexagonal CdS crystal phase (JCPDF 41-1049). Such low peaks could result from the high dispersity of the as-obtained CdS QDs. Other diffraction peaks related to CdS could be overlapped by the diffraction peaks of anatase TiO_2. In addition, the mesoporous C_{60}−CdS/TiO_2, with a low C_{60} content (<2 wt %), did not exhibit C_{60} characteristic diffraction peaks. It could be ascribed to the high dispersity of C_{60} in the framework of CdS/TiO_2, as shown in Supporting Information (SI) Figure S1. For proving the existence of C_{60} after 400 °C calcination, TG was also utilized to analyze to thermal stability of C_{60} in the presence/absence of CdS/TiO_2 framework. As shown in SI Figure S2, the weight loss of C_{60} was observed when the temperature increased to about 400 °C to the case pure C_{60}. In the presence of CdS/TiO_2 framework, only 12 wt % loss was observed before 200 °C to the case of C_{60}−CdS/TiO_2. Such loss was attributed to the removal of water or hydroxyl groups absorbed on the surface of C_{60}−CdS/TiO_2. No obvious weight loss could be observed over 400 °C. Such excellent thermal stability could be attributed to the protection of TiO_2 framework. As known, the thermal conductivity constant of TiO_2 was about 3.8 w/m·k at 400 °C. Upon being calcined at 400 °C, most heat will be absorbed by the framework of TiO_2, thus C_{60} layers will be maintained. These results indicated that the C_{60} molecules could be obtained in the framework of CdS/TiO_2 even after calcination at 400 °C.

Nitrogen adsorption−desorption isotherms were recorded to evaluate the effect of C_{60} on the porous structure of CdS/TiO_2 samples. As shown in Figure 2, all samples exhibited a similar type-IV isotherm, illustrating that these samples possessed mesoporous structure. As shown in Table 1, CdS/TiO_2 sample possessed a specific surface area of 191 $m^2 \cdot g^{-1}$. It clearly indicated that both surface area and pore volume decreased upon increasing the C_{60} content. Such decrease could be ascribed to the occupation of C_{60} clusters in the pore channels of mesoporous structures. These results further suggested that the C_{60} clusters and CdS QDs were embedded in the pore wall of the mesoporous TiO_2 networks. From the BET results, one could draw a conclusion that such mesoporous C_{60}−CdS/TiO_2 architectures remained opened mesoporous channels and had a large surface area. Such structure is highly required for catalyst design, being beneficial to enhance the molecular transport capacity of reactants and the release of H_2.[35]

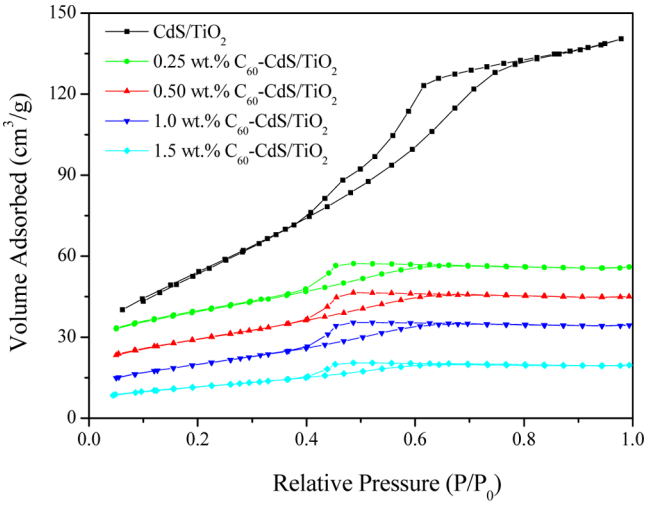

Figure 2. N_2-sorption isotherms of CdS/TiO_2 and C_{60}−CdS/TiO_2 samples.

The transmission electron microscopy (TEM) images were utilized to define the ordered structure and crystal phase of the as-obtained samples. As shown in Figure 3a, a long-range ordered structure was readily observed in the CdS/TiO_2 composites. Upon introducing C_{60}, the long-range ordered structure was still retained except for a slightly twist, as illustrated in Figure 3b. Besides, the nanocrystalline nature of hexagonal CdS and anatase TiO_2 could be well-resolved in the HRTEM image of C_{60}−CdS/TiO_2, as shown in Figure 3c. It was noted that there was no change of lattice structure of TiO_2 (0.352 nm) and CdS (0.316 nm) after embedding C_{60} into the mesoporous framework of TiO_2. It was also found that an amorphous coverture layer was surrounded on the surface of TiO_2 and CdS nanocrystals, and the layer possessed a thickness of 1−2 nm, about 2−3 times of the diameter of C_{60} molecular (0.7 nm). Therefore, it could be estimated that C_{60} clusters were attached with TiO_2 and CdS indicated by the white dot cycles, similar to the previous reports.[36,37] Furthermore, the existence of C, O, S, Cd, and Ti elements of the mesoporous C_{60}−CdS/TiO_2 nanocomposites could also be proven by the EDS analysis (Inset of Figure 3c).

The XPS spectra of the as-obtained CdS/TiO_2 and C_{60}−CdS/TiO_2 are shown in Figure 4. The introduction of C_{60} via the EISA route did not exhibit obvious influence on the principal peak position of the Cd 3d, O 1s, and S 2p peaks, which was an effective evidence to demonstrate the prohibition of sulfide ion oxidation. This could allow the photostability of CdS to be maintained well in the utilization in photocatalytic reaction. Nevertheless, positive shifts of the binding energy of Ti 2p were exhibited at about 0.2 and 0.4 eV for Ti $2p_{3/2}$ and Ti $2p_{1/2}$, indicating the strong interaction between CdS and TiO_2. It should be noted that the C 1s peak at 284.9 eV was assigned to adventitious carbon from the C_{60}.[38,39] The XPS results further suggest the formation of heterojunctions between C_{60} and CdS/TiO_2 in the framework of mesoporous TiO_2.

As is known, the light absorption capability (LAC) played an important role in affecting the photocatalytic activity of the

DOI: 10.1021/am5088665
ACS Appl. Mater. Interfaces 2015, 7, 4533−4540

Table 1. Structural Parameters of All As-Obtained Samples

samples	BET surface area (m^2/g)[a]	pore volume (cm^3/g)[b]	pore size (nm)[c]
CdS/TiO_2	191	0.180	3.4
0.25 wt % C_{60}–CdS/TiO_2	90	0.0604	3.0
0.50 wt % C_{60}–CdS/TiO_2	83	0.0646	2.9
1.0 wt % C_{60}–CdS/TiO_2	71	0.0532	2.9
1.5 wt % C_{60}–CdS/TiO_2	41	0.0304	2.8

[a]BET special surface area calculated from the linear part of the BET plot (p/p_0 = 0.1–0.2). [b]The total pore volumes were estimated from the adsorbed amount at a relative pressure of p/p_0 = 0.99. [c]The pore-size diameters (PSD) were derived from the desorption branches of the isotherms by using the Barrett–Joyner–Halenda (BJH) method.

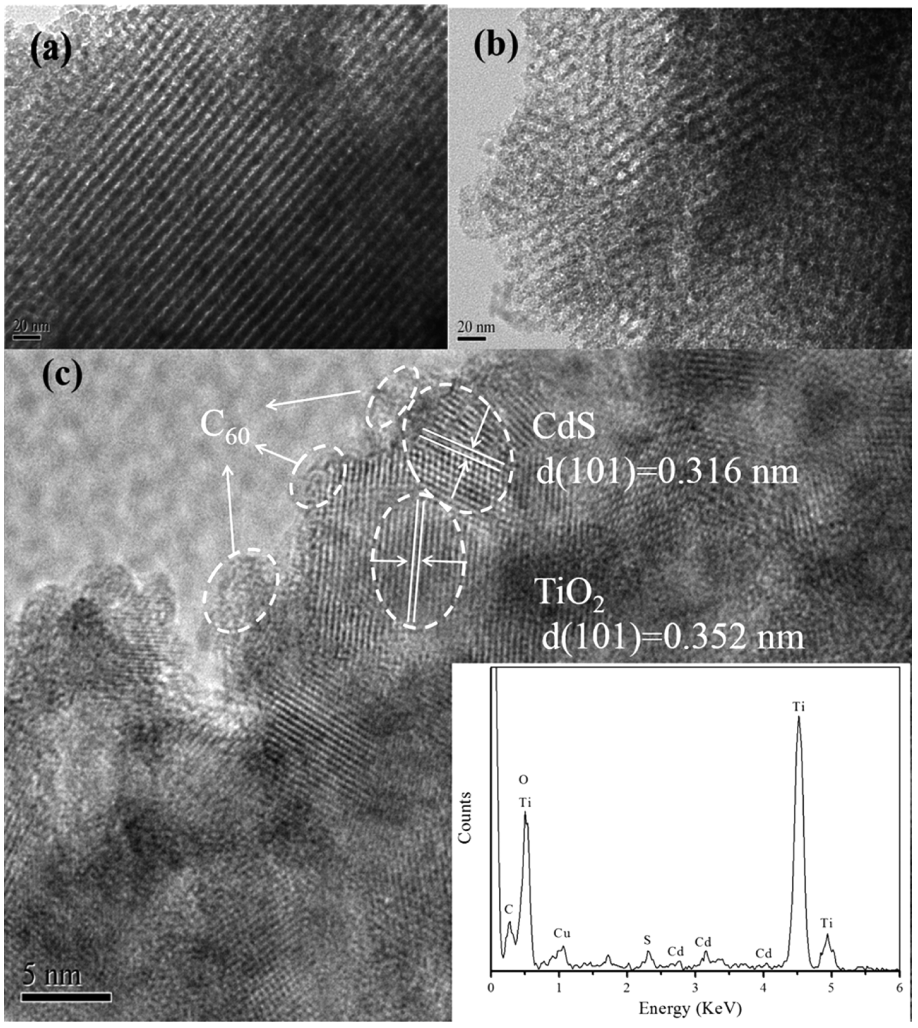

Figure 3. TEM image of CdS/TiO_2 (a), 0.50 wt % C_{60}–CdS/TiO_2 (b), and the HRTEM image and EDS spectrum (inset) of 0.50 wt % C_{60}–CdS/TiO_2 (c).

photocatalysts. Thus, it is highly necessary to keep or improve the LAC of the as-formed CdS/TiO_2 even after loading the C_{60} clusters. In order to evaluate the LAC of samples, UV–visible diffuse reflectance spectroscopy (DRS) was used. As shown in Figure 5a, the as-obtained samples exhibited the typical absorption, ranging from 400 to 550 nm in the visible-light region. It could be assigned to the embedded CdS QDs in the pore wall of mesoporous TiO_2. Such CdS QDs may change the intrinsic band gap absorption of TiO_2. Furthermore, the introduction of the C_{60} clusters into the mesoporous CdS/TiO_2 framework results in to a high LAC in the visible-light region. Interestingly, the as prepared C_{60}–CdS/TiO_2 exhibits the stronger absorption along with the increasing C_{60} content, indicating the increment of surface electric charge and electronic interaction between C_{60} and CdS/TiO_2.[20,40] Such enhanced light adsorption capability owing to the C_{60}-introduction would be highly necessary for making the C_{60}–CdS/TiO_2 mesoporous composites an ideal photocatalyst.

For proving the enhancement of the C_{60} clusters on the photoresponse performance of mesoporous C_{60}–CdS/TiO_2 composites, transient photocurrent techniques were used to measure and evaluate the performance. As shown in Figure 5b, all of the C_{60}–CdS/TiO_2 composites exhibited stronger photocurrents compared with CdS/TiO_2 under visible-light (λ > 420 nm) irradiation at an applied potential of 0.5 V vs SCE. Among all the C_{60}-modified samples, the 0.50 wt % C_{60}–

DOI: 10.1021/am5088665
ACS Appl. Mater. Interfaces 2015, 7, 4533–4540

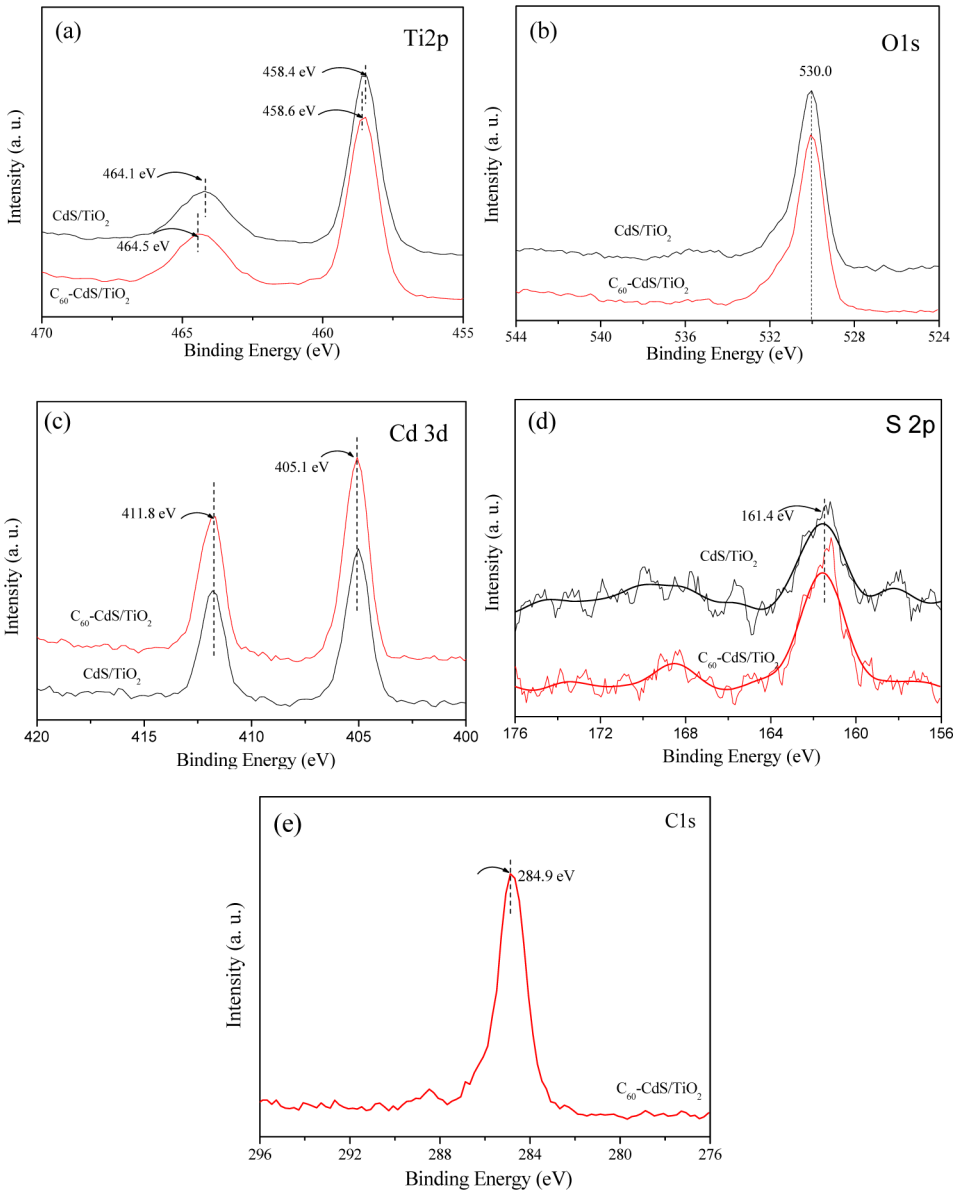

Figure 4. XPS spectra in Ti 2p (a), O 1s (b), Cd 3d (c), S 2p (d) level of CdS/TiO_2 and 0.50 wt % C_{60}−CdS/TiO_2, respectively, and C 1s level (e) of the C_{60}−CdS/TiO_2.

CdS/TiO_2 sample possessed the highest photocurrent density. Nevertheless, further increasing the loaded amount of C_{60} clusters resulted in the decrease of photocurrent density. This could be attributed to the light shielding effect of excess C_{60} coverage on the surface CdS/TiO_2, although the light absorption capability could still be increased upon introducing excess C_{60}, suggested by the UV−vis results (Figure 5a). It should also be noted that photocurrent responses were highly reproducible for numerous on−off cycles and remained stable. As for the 0.50 wt % C_{60}−CdS/TiO_2 sample, C_{60} clusters as the electron acceptor greatly enhanced the photogenerated electrons transfer velocity from the conduction band of both CdS and TiO_2 to C_{60} clusters based on the photocurrent results. It could effectively prohibit the direct recombination of photoinduced electrons and holes, allowing more electrons to be captured by protons to from H_2. Such low electron-hole recombination rates can also be supported by the photoluminescence results. Both CdS/TiO_2 and 0.50 wt % C_{60}−CdS/TiO_2 displayed peaks at around 560 nm, as shown in Figure 5c. An obvious fluorescence peak decrease can be observed after introducing C_{60} clusters. Such decrease of fluorescence indicated the low recombination rate of photogenerated electrons and holes in the C_{60}−CdS/TiO_2 samples, as well as a favorable (or close) contact among C_{60}, TiO_2, and CdS.[41,42] In addition, a time-resolved absorption spectrum was also utilized to trace the lifetime of the photogenerated charge carries.[43,44] It was proven that C_{60} could prolong the lifetime of charge on semiconductors,[43] thus the C_{60} cluster protection layers could greatly accelerate the photogenerated electron transfer of CdS/TiO_2 composites. On the basis of the above results, it could be acknowledged that the photogenerated electron fast transfer rate owing to the excellent conductivity of C_{60} clusters would be favorable for both the enhancement of the photocatalytic activity of C_{60}−CdS/TiO_2 for H_2 evolution and the prohibition of photocorrosion of CdS, not allowing the reduction of cadmium ions.

For testing the photocatalytic performance of the as-obtained samples, photocatalytic H_2 evolution was utilized as the probe

DOI: 10.1021/am5088665
ACS Appl. Mater. Interfaces 2015, 7, 4533−4540

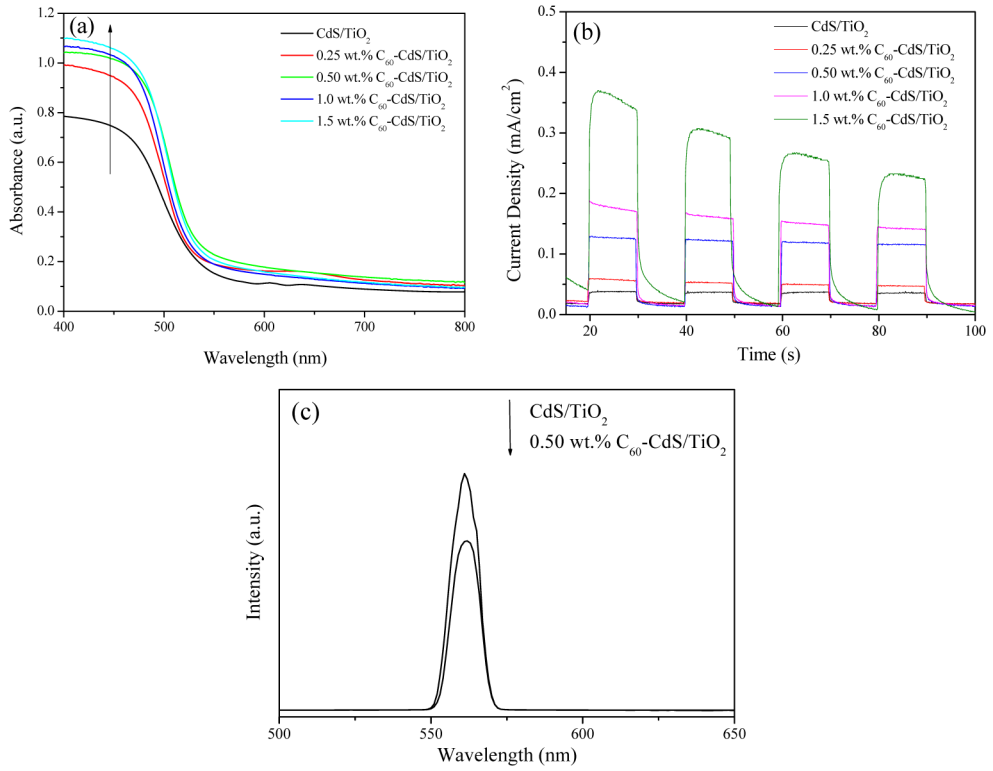

Figure 5. UV−vis spectra (a), photocurrent density measured at 0.5 V vs SCE under chopped (on−off and a pluse of 10 s) 300 W Xe lamp (λ > 420 nm) in a 0.5 M aqueous Na_2SO_4 electrolyte (b) of CdS/TiO_2 and C_{60}−CdS/TiO_2 samples, and photoluminescence spectra (c) of CdS/TiO_2 and 0.50 wt % C_{60}−CdS/TiO_2 excited by 280 nm.

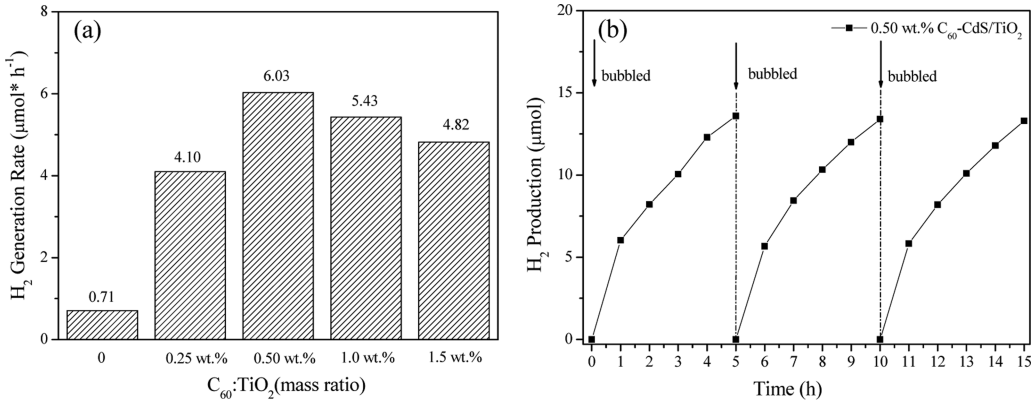

Figure 6. (a) Photocatalytic activities of the different amount of C_{60} in C_{60}−CdS/TiO_2. (b) Recycling test of the 0.50 wt % C_{60}−CdS/TiO_2 for H_2 evolution rate in aqueous solution under visible-light (λ = 420 nm) LED light irradiation.

reaction by using a mixed Na_2S−Na_2SO_3 aqueous solution system in the absence of cocatalyst (noble metal Pt). As shown in Figure 6a, CdS/TiO_2 exhibited a low photocatalytic activity for H_2 evolution rate (0.71 μmol·h^{-1}). Upon loading C_{60} clusters, the H_2 evolution rate was greatly enhanced. The sample of 0.50 wt % C_{60}−CdS/TiO_2 exhibited the highest H_2 evolution rate of about 6.03 μmol·h^{-1}, with about 2.0% of QE under visible light irradiation (4 × 3 W LEDs, single wavelength at 420 nm). Further increasing C_{60} loaded amount over 0.50 wt % resulted in a lower H_2 evolution rate. Such decrease could be attributed to the light shielding effect, resulting from the over loaded C_{60} layers. Such effect could not allow light to reach the surface of the CdS/TiO_2. These results related to activities were similar to the photocurrent results. For further proving the enhancement effect of C_{60}, C_{60}/CdS (with various C_{60} contents) samples were also prepared as comparative candidates. The mass ratio of C_{60}/CdS was tuned from 0 to 1.5%, same to the mass ratio of C_{60}/TiO_2. From SI Figure S3, it could be observed that the optimal ratio of C_{60}/CdS (0.5 wt %) resulted in a hydrogen evolution rate of about 0.11 μmol·h^{-1}, about four times of that of CdS. These results further proved that C_{60} could accelerate the separation of photogenerated electrons for H_2 evolution. As a good photocatalyst for H_2 evolution, the stability played an important role for evaluating its photocatalytic performance. Herein, the sample of 0.50 wt % C_{60}−CdS/TiO_2 was repeated for H_2 evolution from water-splitting via recovering catalysts through centrifugation. As shown in Figure 6b, the H_2 evolution rate of the as-obtained sample could be well maintained even after three times of usage. The remaining reaction solution after

DOI: 10.1021/am5088665
ACS Appl. Mater. Interfaces 2015, 7, 4533−4540

reuse was also centrifuged and analyzed with ICP. The results indicated that nearly no cadmium ions were detected. For proving the promotion effect of C_{60} on the stability of CdS/TiO_2 during the H_2 evolution, the recyclability of pure CdS/TiO_2 was also investigated. As shown in SI Figure S4, an obvious decrease was observed after 10 h of reaction, suggesting that C_{60} played an important role for enhancing both the activity and stability of the CdS/TiO_2 composites. Such excellent stability could be ascribed to the strong antiphotocorrosion effect resulted from the protection layer of C_{60} clusters.

A proposed schematic mechanism for the high H_2 evolution activity of C_{60}−CdS/TiO_2 is illustrated in Figure 7. Under

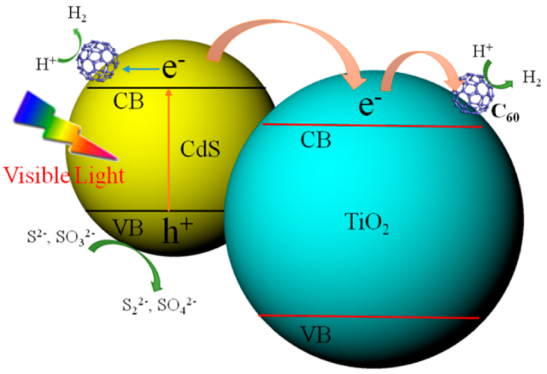

Figure 7. Schematic illustration of the charge transfer of C_{60}−CdS/TiO_2 composites working under visible-light irradiation.

visible-light illumination, the electrons on the valence band (VB) of CdS could be excited to the conduction band (CB), leaving holes in the VB. And these CB electrons can be further injected into the CB of TiO_2.[11] Meanwhile, C_{60} was regarded as an electron acceptor, and its special electron structure allowed rapid electron transfer to reduce the combination rate of the photoinduced electrons and holes pairs. Thus, the loaded C_{60} clusters could act as electron transit stations for both fast trapping electrons from the CdS/TiO_2 composites and serving as H_2 evolution sites for adsorbing and reducing H^+ ions.

4. CONCLUSIONS

C_{60}−CdS/TiO_2 were prepared using a novel method by preplanting crystal seeds (C_{60} and CdO) into the pore wall of ordered mesoporous TiO_2, accompanied by an ion-exchange route for tuning CdO to CdS. Such C_{60}−CdS/TiO_2 photocatalyst presented excellent photocatalytic activity during the water-splitting for H_2 evolution under visible-light irradiation (λ = 420 nm) and remarkable photostability owing to the presence of C_{60} cluster protecting layers in the TiO_2 framework. C_{60} layers effectively enhanced the light absorption capability of the prepared catalysts and greatly accelerated the photogenerated electron transfer velocity with the formation of antiphotocorrosion of CdS. Besides, they could also act as the electron transit stations for both fast trapping electrons from the CdS/TiO_2 composites and serve as H_2 evolution sites for adsorbing and reducing H^+ ions.

■ ASSOCIATED CONTENT

Ⓢ Supporting Information

XRD patterns of different content of C_{60} in C_{60}−CdS/TiO_2, TG analysis, H_2 photocatalytic evolution of C_{60}/CdS samples, and the recyclability of mesoporous CdS/TiO_2 for H_2 photocatalytic evolution. This material is available free of charge via the Internet at http://pubs.acs.org/.

■ AUTHOR INFORMATION

Corresponding Authors

*E-mail: dqzhang@shnu.edu.cn (D.Z.).
*E-mail: Liguisheng@shnu.edu.cn (G.L.).

Author Contributions

†Equal contribution.

Notes

The authors declare no competing financial interest.

■ ACKNOWLEDGMENTS

This work was supported by the National Natural Science Foundation of China (21207090, 21477079, and 21237003), Shanghai Government (15QA1403300, 11SG42, 11ZR1426300, 13YZ054, and 14ZR1430900), PCSIRT (IRT1269), Doctoral Program by Higher Education (2012312712009), and by a scheme administrated by Shanghai Normal University (S30406).

■ REFERENCES

(1) Schlapbach, L.; Zuttel, A. Review Article Hydrogen-Storage Materials for Mobile Applications. *Nature* **2001**, *414*, 353−358.
(2) Churchard, A. J.; Banach, E.; Borgschulte, A.; Caputo, R.; Chen, J. C.; Clary, D. C.; Fijalkowski, K. J.; Geerlings, H.; Genova, R. V.; Grochala, W.; Jaron, T.; Juanes-Marcos, J. C.; Kasemo, B.; Kroes, G.-J.; Ljubic, I.; Naujoks, N.; Norskov, J. K.; Olsen, R. A.; Pendolino, F.; Remhof, A.; Romanszki, L.; Tekin, A.; Vegge, T.; Zach, M.; Zuettel, A. A Multifaceted Approach to Hydrogen Storage. *Phys. Chem. Chem. Phys.* **2011**, *13*, 16955−16972.
(3) Xiang, Q.; Yu, J.; Jaroniec, M. Enhanced Photocatalytic H_2 Production Activity of Graphene-Modified Titania Nanosheets. *Nanoscale* **2011**, *3*, 3670−3678.
(4) Fujishima, A.; Honda, K. Electrochemical Photolysis of Water at a Semiconductor Electrode. *Nature* **1972**, *238*, 37−38.
(5) Li, Q.; Guo, B.; Yu, J.; Ran, J.; Zhang, B.; Yan, H.; Gong, J. R. Highly Efficient Visible-Light-Driven Photocatalytic Hydrogen Production of CdS-Cluster-Decorated Graphene Nanosheets. *J. Am. Chem. Soc.* **2011**, *133*, 10878−10884.
(6) Yu, J.; Yu, Y.; Zhou, P.; Xiao, W.; Cheng, B. Morphology-dependent photocatalytic H_2-production activity of CdS. *Appl. Catal., B* **2014**, *156*−*157*, 184−191.
(7) Li, X.; Jia, Y.; Cao, A. Tailored Single-Walled Carbon Nanotube-CdS Nanoparticle Hybrids for Tunable Optoelectronic Devices. *ACS Nano* **2010**, *4*, 506−512.
(8) Pan, Z.; Zhang, H.; Cheng, K.; Hou, Y.; Hua, J.; Zhong, X. Highly Efficient Inverted Type-I CdS/CdSe Core/Shell Structure QD-Sensitized Solar Cells. *ACS Nano* **2012**, *6*, 3982−3991.
(9) Ferancova, A.; Rengaraj, S.; Kim, Y.; Labuda, J.; Sillanpaa, M. Electrochemical Determination of Guanine and Adenine by CdS Microspheres Modified Electrode and Evaluation of Damage to DNA Purine Bases by UV Radiation. *Biosens. Bioelectron.* **2010**, *26*, 314−320.
(10) Li, Z. J.; Wang, J. J.; Li, X. B.; Fan, X. B.; Meng, Q. Y.; Feng, K.; Chen, B.; Tung, C. H.; Wu, L. Z. Photocatalysis: An Exceptional Artificial Photocatalyst, NiH−CdSe/CdS Core/Shell Hybrid, Made In Situ from CdSe Quantum Dots and Nickel Salts for Efficient Hydrogen Evolution. *Adv. Mater.* **2014**, *25*, 6634−6634.
(11) Li, G. S.; Zhang, D. Q.; Yu, J. C. A New Visible-Light Photocatalyst: CdS Quantum Dots Embedded Mesoporous TiO_2. *Environ. Sci. Technol.* **2009**, *43*, 7079−7085.
(12) Ke, D. N.; Liu, S. L.; Dai, K.; Zhou, J. P.; Zhang, L. N.; Peng, T. Y. CdS/Regenerated Cellulose Nanocomposite Films for Highly Efficient Photocatalytic H_2 Production under Visible Light Irradiation. *J. Phys. Chem. C* **2009**, *113*, 16021−16026.

DOI: 10.1021/am5088665
ACS Appl. Mater. Interfaces 2015, 7, 4533−4540

(13) Kudo, A.; Miseki, Y. Heterogeneous Photocatalyst Materials for Water Splitting. *Chem. Soc. Rev.* **2009**, *38*, 253−278.
(14) Hu, Y.; Gao, X.; Yu, L.; Wang, Y.; Ning, J.; Xu, S.; Lou, X. W. Carbon-Coated CdS Petalous Nanostructures with Enhanced Photostability and Photocatalytic Activity. *Angew. Chem., Int. Ed.* **2013**, *125*, 5746−5749.
(15) Zhang, J.; Qiao, S. Z.; Qi, L.; Yu, J. Fabrication of NiS Modified CdS Nanorod p−n Junction Photocatalysts with Enhanced Visible-Light Photocatalytic H_2-Production Activity. *Phys. Chem. Chem. Phys.* **2013**, *15*, 12088−12094.
(16) Ding, L.; Zhou, H.; Lou, S.; Ding, J.; Zhang, D.; Zhu, H.; Fan, T. Butterfly Wing Architecture Assisted CdS/Au/TiO_2 Z-Scheme Type Photocatalytic Water Splitting. *Int. J. Hydrogen Energy* **2013**, *38*, 8244−8253.
(17) Yu, J. G.; Ma, T. T.; Liu, S. W. Enhanced Photocatalytic Activity of Mesoporous TiO_2 Aggregates by Embedding Carbon Nanotubes as Electron-Transfer Channel. *Phys. Chem. Chem. Phys.* **2011**, *13*, 3491−3501.
(18) Dai, K.; Peng, T.; Ke, D.; Wei, B. Photocatalytic Hydrogen Generation Using a Nanocomposite of Multi-walled Carbon Nanotubes and TiO_2 Nanoparticles under Visible Light Irradiation. *Nanotechnology* **2009**, *20*, 125603.
(19) An, G.; Ma, W.; Sun, Z.; Liu, Z.; Han, B.; Miao, S.; Miao, Z.; Ding, K. Preparation of Titania/Carbon Nanotube Composites Using Supercritical Ethanol and Their Photocatalytic Activity for Phenol Degradation under Visible Light Irradiation. *Carbon* **2007**, *45*, 1795−1801.
(20) Silva, C. G.; Faria, J. L. Photocatalytic Oxidation of Benzene Derivatives in Aqueous Suspensions: Synergic Effect Induced by the Introduction of Carbon Nanotubes in a TiO_2 Matrix. *Appl. Catal., B* **2010**, *101*, 81−89.
(21) Zhou, W.; Pan, K.; Qu, Y.; Sun, F.; Tian, C.; Ren, Z.; Tian, G.; Fu, H. Photodegradation of Organic Contamination in Wastewaters by Bonding TiO_2/Single-Walled Carbon Nanotube Composites with Enhanced Photocatalytic Activity. *Chemosphere* **2010**, *81*, 555−561.
(22) Li, N.; Ma, Y.; Wang, B.; Huang, Y.; Wu, Y.; Yang, X.; Chen, Y. Synthesis of Semiconducting SWNTs by Arc Discharge and Their Enhancement of Water Splitting Performance with TiO_2 Photocatalyst. *Carbon* **2011**, *49*, 5132−5141.
(23) Yu, J.; Ma, T.; Liu, G.; Cheng, B. Enhanced Photocatalytic Activity of Bimodal Mesoporous Titania Powders by C-60 Modification. *Dalton Trans.* **2011**, *40*, 6635−6644.
(24) Fan, W.; Lai, Q.; Zhang, Q.; Wang, Y. Nanocomposites of TiO_2 and Reduced Graphene Oxide as Efficient Photocatalysts for Hydrogen Evolution. *J. Phys. Chem. C* **2011**, *115*, 10694−10701.
(25) Xiang, Q.; Yu, J.; Jaroniec, M. Enhanced Photocatalytic H_2-Production Activity of Graphene-Modified Titania Nanosheets. *Nanoscale* **2011**, *3*, 3670−3678.
(26) Jiang, G.; Lin, Z.; Chen, C.; Zhu, L.; Chang, Q.; Wang, N.; Wei, W.; Tang, H. TiO_2 Nanoparticles Assembled on Graphene Oxide Nanosheets with High Photocatalytic activity for Removal of Pollutants. *Carbon* **2011**, *49*, 2693−2701.
(27) Fu, H.; Xu, T.; Zhu, S.; Zhu, Y. Photocorrosion Inhibition and Enhancement of Photocatalytic Activity for ZnO via Hybridization with C_{60}. *Environ. Sci. Technol.* **2008**, *42*, 8064−8069.
(28) Yu, G.; Gao, J.; Hummelen, J. C.; Wudl, F.; Heeger, A. J. Polymer Photovoltaic Cells: Enhanced Efficiencies via a Network of Internal Donor−Acceptor Heterojunctions. *Science* **1995**, *270*, 1789−1791.
(29) Li, G.; Jiang, B.; Li, X.; Lian, Z.; Xiao, S.; Zhu, J.; Zhang, D.; Li, H. C_{60}/$Bi_2TiO_4F_2$ Heterojunction Photocatalysts with Enhanced Visible-Light Activity for Environmental Remediation. *ACS Appl. Mater. Interfaces* **2013**, *5*, 7190−7197.
(30) Dai, K.; Yao, Y.; Liu, H.; Mohamed, I.; Chen, H.; Huang, Q. Enhancing the Photocatalytic Activity of Lead Molybdate by Modifying with Fullerene. *J. Mol. Catal. A: Chem.* **2013**, *374*−*375*, 111−117.
(31) Hassan, N.; Holze, R. A Comparative Electrochemical Study of Electrosorbed 2- and 4-Mercaptopyridines and Their Application as Corrosion Inhibitors at C_{60} Steel. *J. Chem. Sci.* **2009**, *121*, 693−701.
(32) Yu, J. G.; Qi, L. F.; Jaroniec, M. Hydrogen Production by Photocatalytic Water Splitting over Pt/TiO_2 Nanosheets with Exposed (001) Facets. *J. Phys. Chem. C* **2010**, *114*, 13118−13125.
(33) Li, H. X.; Bian, Z. F.; Zhu, J.; Huo, Y. N.; Li, H.; Lu, Y. F. Mesoporous Au/TiO_2 Nanocomposites with Enhanced Photocatalytic Activity. *J. Am. Chem. Soc.* **2007**, *129*, 4538−4539.
(34) Yang, H. G.; Sun, C. H.; Qiao, S. Z.; Zou, J.; Liu, G.; Smith, S. C.; Cheng, H. M.; Lu, G. Q. Anatase TiO_2 Single Crystals with a Large Percentage of Reactive Facets. *Nature* **2008**, *453*, 638−641.
(35) Yu, J. C.; Li, G. S.; Wang, X. C.; Hu, X. L.; Leung, C. W.; Zhang, Z. D. An Ordered Cubic Im3m Mesoporous Cr−TiO_2 Visible Light Photocatalyst. *Chem. Commun.* **2006**, 2717−2719.
(36) Amer, M. S.; Busbee, J. D. Self-Assembled Hierarchical Structure of Fullerene Building Blocks; Single-Walled Carbon Nanotubes and C_{60}. *J. Phys. Chem. C* **2011**, *115*, 10483−10488.
(37) Kratschmer, W.; Lamb, L. D.; Fostiropoulos, K.; Huffman, D. R. Solid C_{60}: A New Form of Carbon. *Nature* **1990**, *347*, 354−358.
(38) Wang, F.; Zhang, K. Physicochemical and Photocatalytic Activities of Self-Assembling TiO_2 Nanoparticles on Nanocarbons Surface. *Curr. Appl. Phys.* **2012**, *12*, 346−352.
(39) Liu, B.; Zeng, H. C. Carbon Nanotubes Supported Mesoporous Mesocrystals of Anatase TiO_2. *Chem. Mater.* **2008**, *20*, 2711−2718.
(40) Wang, W. D.; Serp, P.; Kalck, P.; Luís Faria, J. Photocatalytic Degradation of Phenol on MWNT and Titania Composite Catalysts Prepared by a Modified Sol-Gel Method. *Appl. Catal., B* **2005**, *56*, 305−312.
(41) Cheng, B.; Le, Y.; Yu, J. Preparation and Enhanced Photocatalytic Activity of Ag@TiO_2 Core-Shell Nanocomposite Nanowires. *J. Hazard. Mater.* **2010**, *177*, 971−977.
(42) Yu, J. G.; Xiong, J.; Cheng, B.; Liu, S. Fabrication and Characterization of Ag-TiO_2 Multiphase Nanocomposite Thin Films with Enhanced Photocatalytic Activity. *Appl. Catal., B* **2005**, *60*, 211−221.
(43) Stewart, M. H.; Huston, A. L.; Scott, A. M.; Oh, E.; Algar, W. R.; Deschamps, J. R.; Susumu, K.; Jain, V.; Prasuhn, D. E.; Blanco-Canosa, J.; Dawson, P. E.; Medintz, I. L. Competition between Förster Resonance Energy Transfer and Electron Transfer in Stoichiometrically Assembled Semiconductor Quantum Dot−Fullerene Conjugates. *ACS Nano* **2013**, *7*, 9489−9505.
(44) Jing, L.; Cao, Y.; Cui, H.; Durrant, J. R.; Tang, J.; Liu, D.; Fu, H. Acceleration Effects of Phosphate Modification on the Decay Dynamics of Photo-Generated Electrons of TiO_2 and Its Photocatalytic Activity. *Chem. Commun.* **2012**, *48*, 10775−10777.

DOI: 10.1021/am5088665
ACS Appl. Mater. Interfaces 2015, 7, 4533−4540